Electronic Supplementary Information (ESI)

Vacancy Engineering of $Cu_{2-x}Se$ Nanoparticles with Tunable LSPR and Magnetism for Dual-modal Imaging Guided Photothermal Therapy of Cancer

Shaohua Zhang,[abd] Qian Huang,[a] Lijuan Zhang,[b] Hao Zhang,[a] Yaobao Han,[a] Qiao Sun,[a] Zhenxiang Cheng,[b] Huizhu Qin,[c] Shixue Dou[b] and Zhen Li*[ab]

a. *Center for Molecular Imaging and Nuclear Medicine, School for Radiological and Interdisciplinary Sciences (RAD-X), Soochow University, Collaborative Innovation Center of Radiation Medicine of Jiangsu Higher Education Institutions, Suzhou 215123, China. Email: zhenli@suda.edu.cn*

b. *Institute for Superconducting and Electronic Materials, Australian Institute for Innovative Materials, University of Wollongong, Wollongong NSW 2522, Australia.*

c. *Medical School of Nantong University, Clinical Medicine, Nantong 226019, China*.

d. *School of Electrical and Electronic Engineering, Nanyang Technological University 50 Nanyang Avenue, Singapore 639798*

Calculation of the photothermal conversion efficiency

$Cu_{2-x}Se$ NPs and different PEGylated CuFeSe NPs were prepared and their concentration was adjusted to have the identical absorbance at 808 nm as shown in Figure S14a. For each sample, 1 mL of NPs solution was loaded into a cuvette and irradiated with a 808-nm laser, followed by natural cooling after the laser was turned off. The monitored temperature profile of each sample is shown in Figure S14b. The photothermal conversion efficiency (η) is calculated according to the following equation.[1]

$$\eta = \frac{m \cdot c \cdot (T_{max} - T_{max,H_2O})}{I \cdot (1 - 10^{-A}) \cdot \tau_s} \quad \textbf{(S1)}$$

where m is the solution mass and equal to 1.0 g in the current study, c is the heat capacity of water and equal to 4.2 J/g, T_{max} and $T_{max,\ H2O}$ are the maximum temperatures of nanoparticle solution and water, respectively. I is the laser power density and equal to 0.75 W/cm^2 in the current study, A is the absorbance of nanoparticle solution at 808 nm and equal to 0.41, and τ_s is the system time constant which can be caculated according to the linear regression of the cooling profile (Figure S14c-f). The photothermal conversion efficiencies of $Cu_{2-x}Se$ NPs and PEGylated CuFeSe NPs obtained from different molar ratios of $Cu_{2-x}Se$: $FeCl_3$ (*i.e.*, 1: 1.5, 1: 3, and 1: 6) are calculated to be 38.3 %, 49.4 %, 42.9 % and 35.8 %, respectively (Table 1). The results demonstrate that enhanced photothermal conversion efficiency can be achieved by optimizing the molar ratio of $Cu_{2-x}Se$: $FeCl_3$.

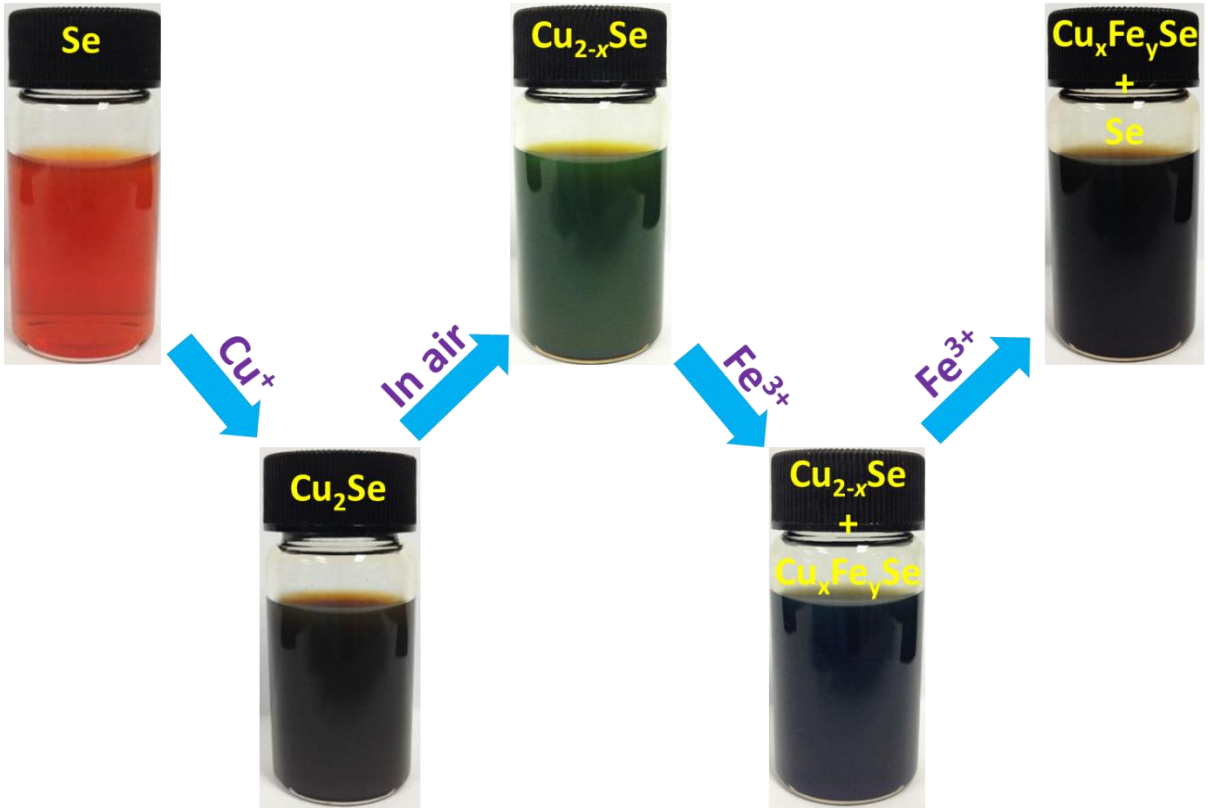

Figure S1. Optical photographs of aqueous dispersions of different samples.

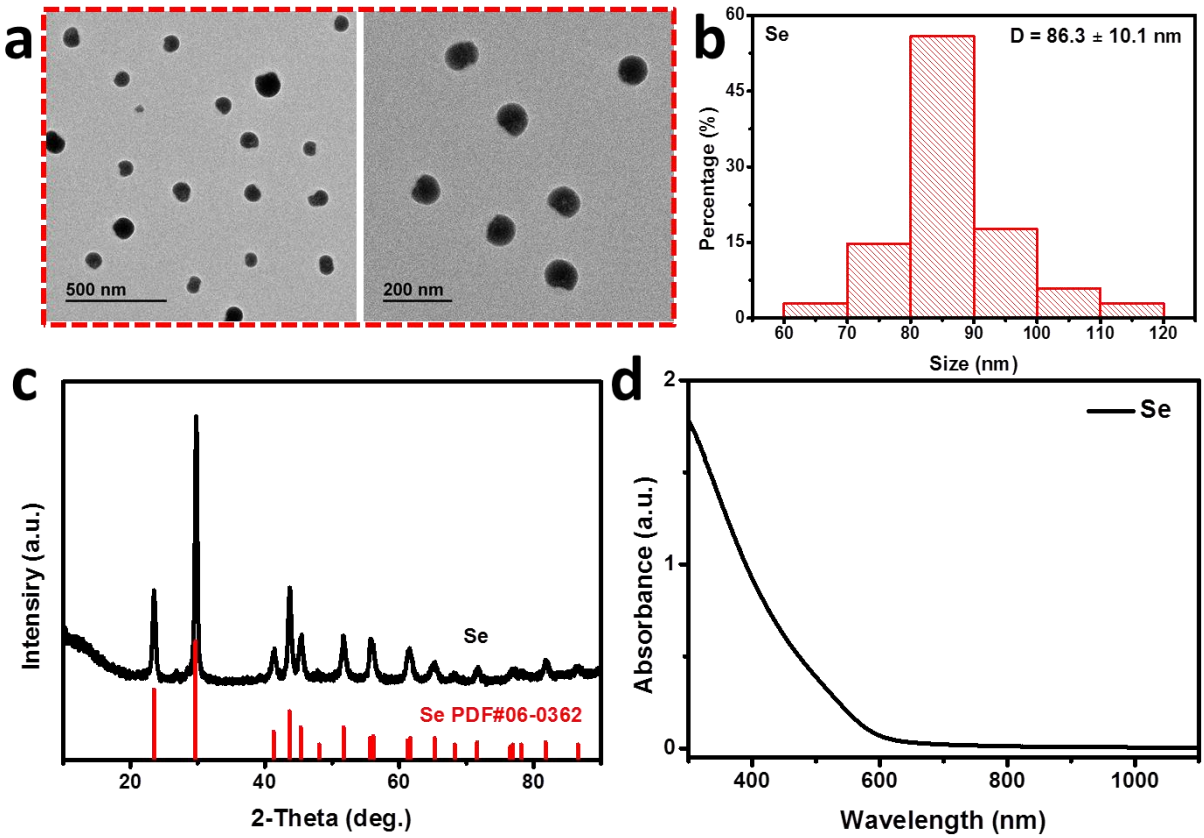

Figure S2. The characterization of Se nanoparticles: (a) TEM images at different magnifications, and (b) the corresponding size distribution histogram. (c) XRD pattern and (d) UV spectrum.

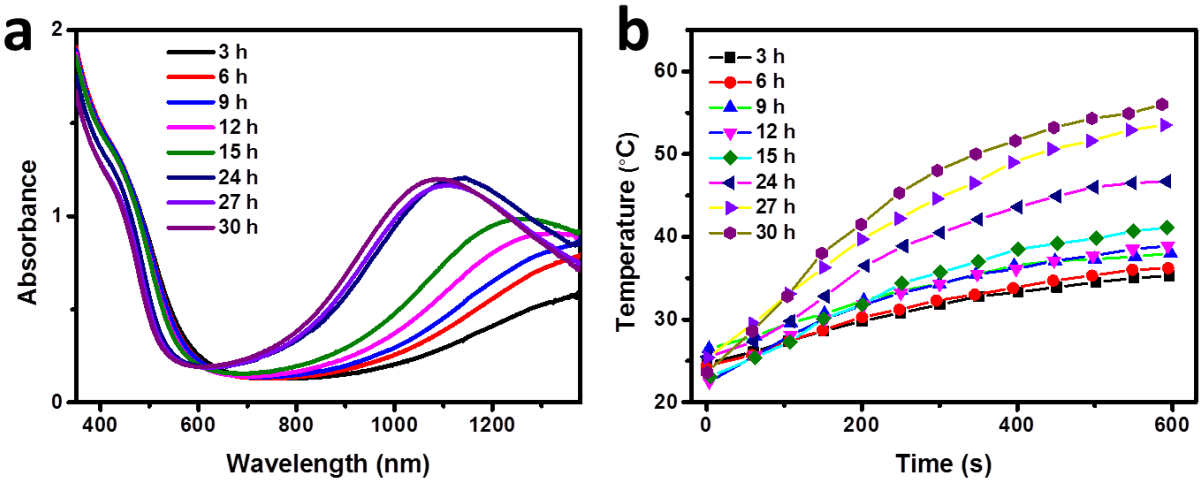

Figure S3. (a) Ultraviolet-visible-near-infrared (UV-vis-NIR) absorption spectra of the formation and evolution of $Cu_{2-x}Se$ sample, and (b) corresponding photothermal heating curves of $Cu_{2-x}Se$ samples.

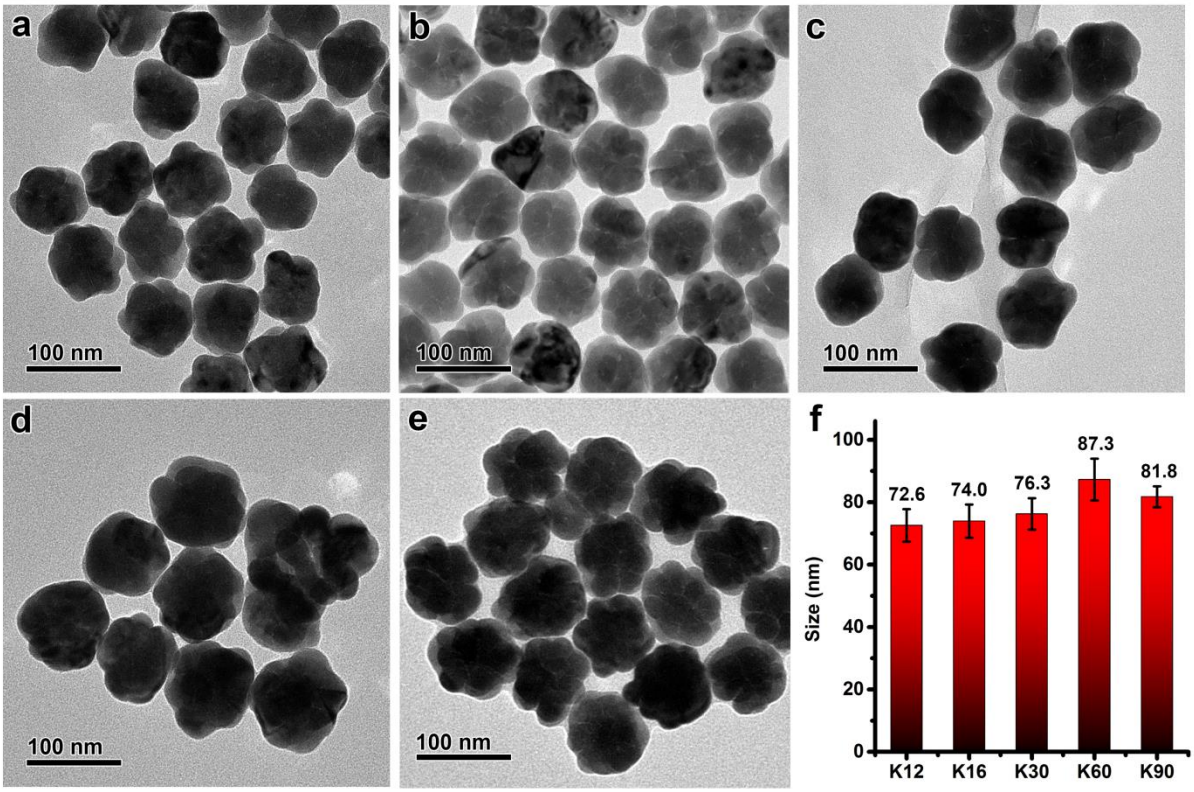

Figure S4. TEM images of $Cu_{2-x}Se$ NPs stabilized by (a) PVP-K12 (MW = 3500), (b) PVP-K16 (MW = 8000), (c) PVP-K30 (MW = 40,000), (d) PVP-K60 (MW = 160,000), (e) PVP-K90 (MW = 360,000); and (f) their size obtained by counting 100 particles of each sample.

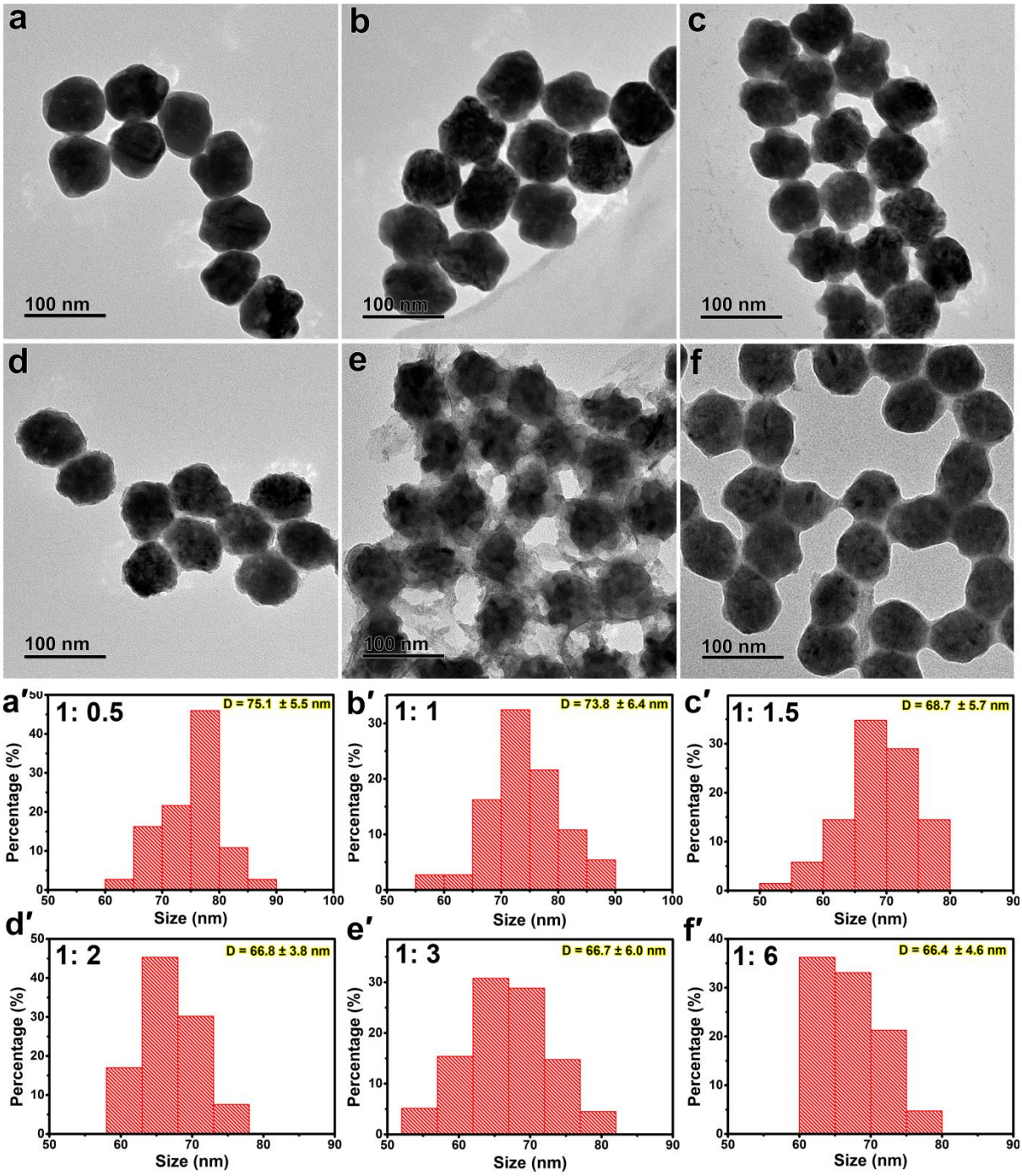

Figure S5. TEM images and corresponding size distributions of the nanostructures obtained with different $Cu_{2-x}Se$: $FeCl_3$ molar ratios: (a and a′) 1: 0.5, (b and b′) 1: 1, (c and c′) 1: 1.5, (d and d′) 1: 2, (e and e′) 1: 3, and (f and f′) 1: 6, at room temperature without Vc and PVP.

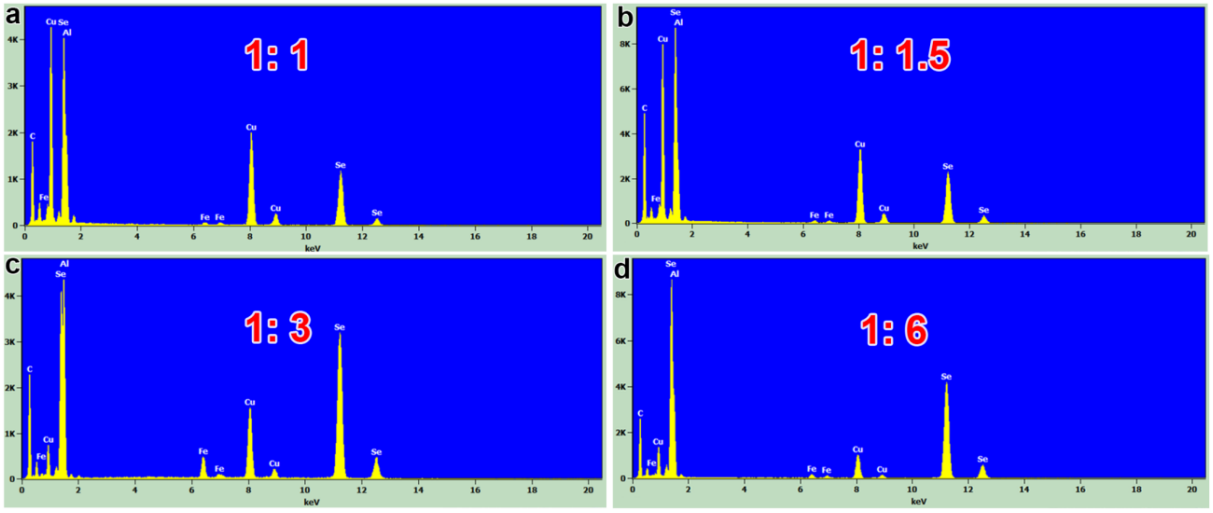

Figure S6. EDS spectra for different Fe^{3+}-doped NPs deposited on carbon-coated aluminium grids: (a) 1: 1, (b) 1: 1.5, (c) 1: 3, (d) 1:6.

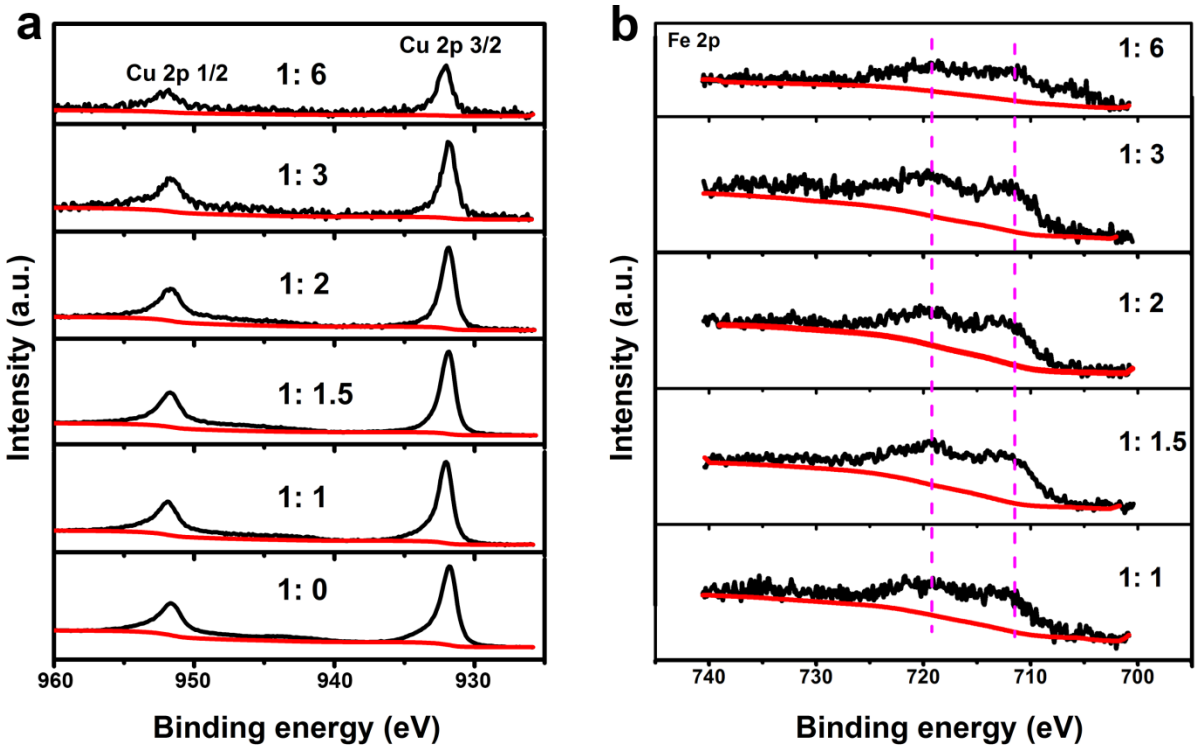

Figure S7. High resolution XPS spectra of (a) Cu 2p and (b) Fe 2p from the different as-synthesized Fe^{3+}-doped NPs.

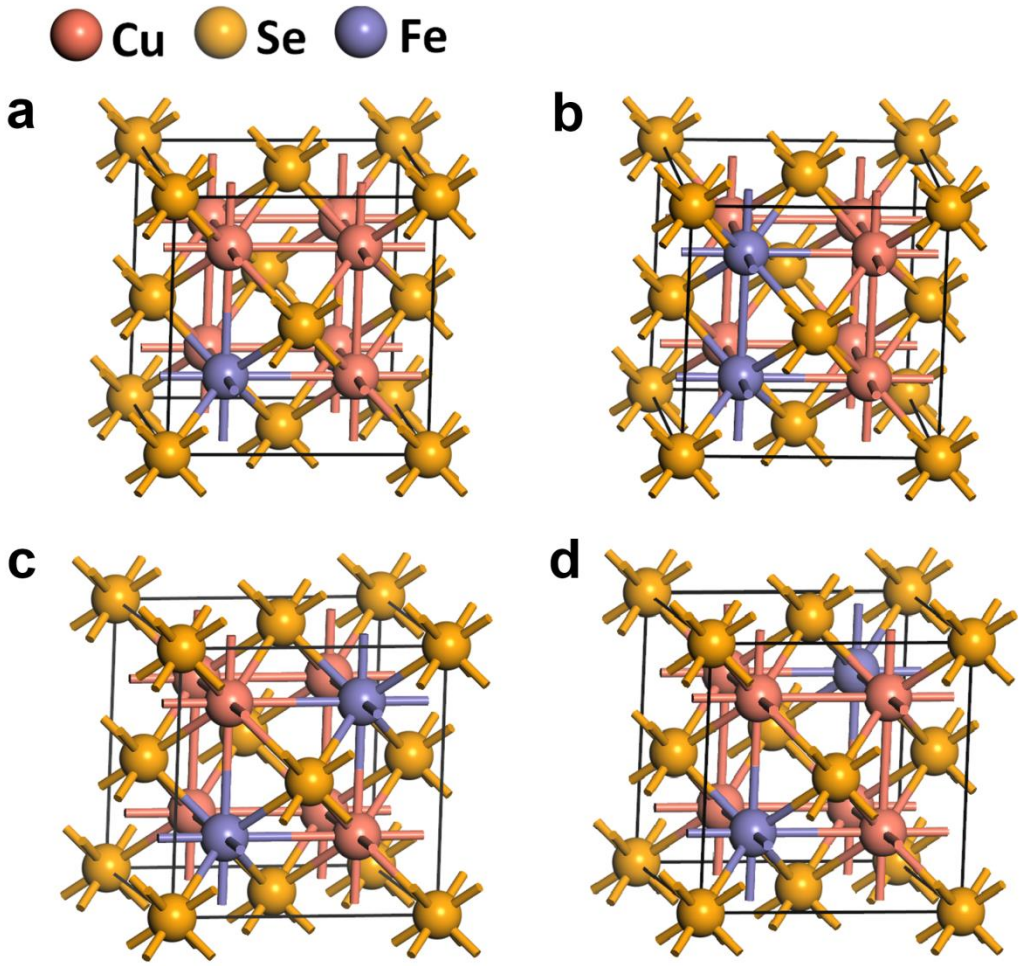

Figure S8. The optimized structures in their ground states of (a) Fe occupying the vacancy of $Cu_{2-x}Se$, and (b-d) Fe replacing Cu atoms at different positions of $Cu_{2-x}Se$.

Figure S9. Optical images of different samples prepared by oxidation and reaction with $FeCl_3$.

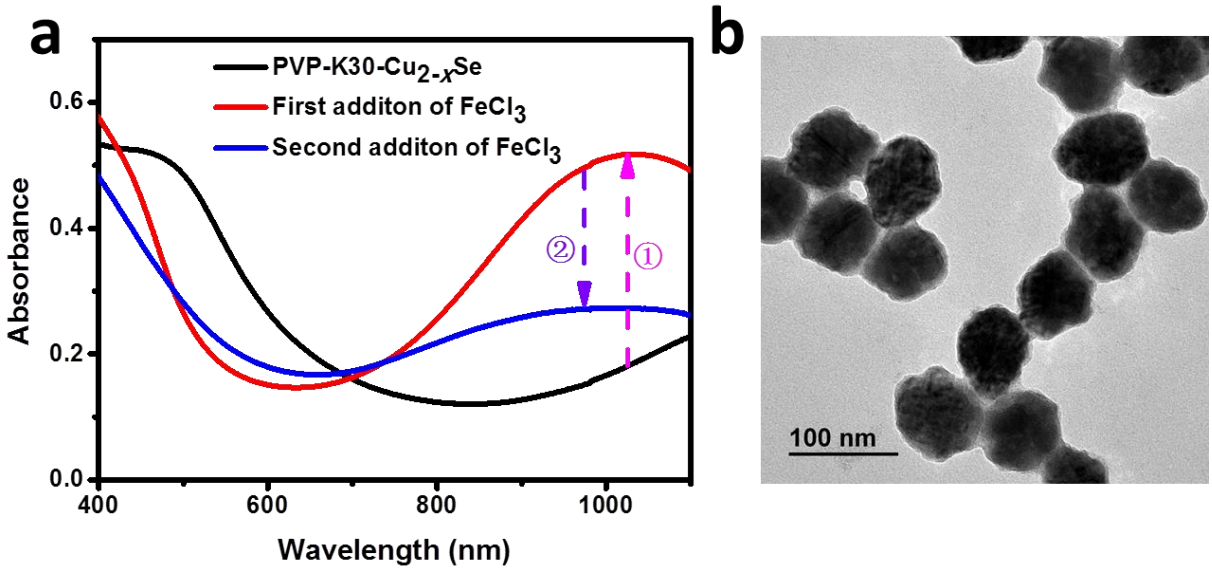

Figure S10. (a) The evolution of UV-vis-NIR absorbance spectra of samples reacted with $FeCl_3$, (b) TEM image of the final sample after the second addition of $FeCl_3$ (molar ratio of Cu_2Se: total amount of $FeCl_3$ is 1: 2).

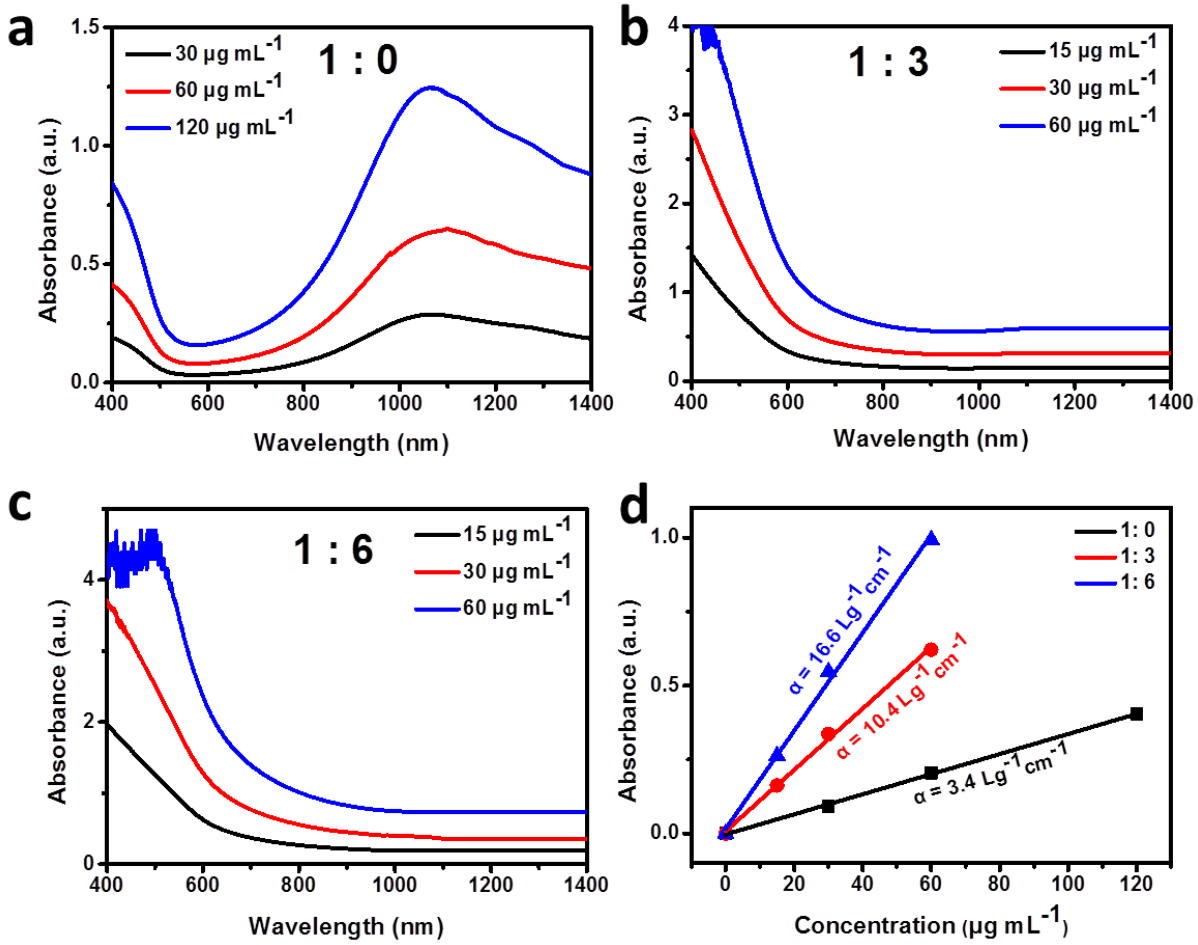

Figure S11. UV-vis-NIR absorbance of $Cu_{2-x}Se$ nanoparticles (a) and hybrid nanoparticles obtained from different $Cu_{2-x}Se$: $FeCl_3$ ratios, *i.e.*, (b) 1: 3; (c) 1: 6. (d) Linear fitting plots of their UV-vis-NIR absorbance *versus* NPs concentration in aqueous solutions at 808 nm.

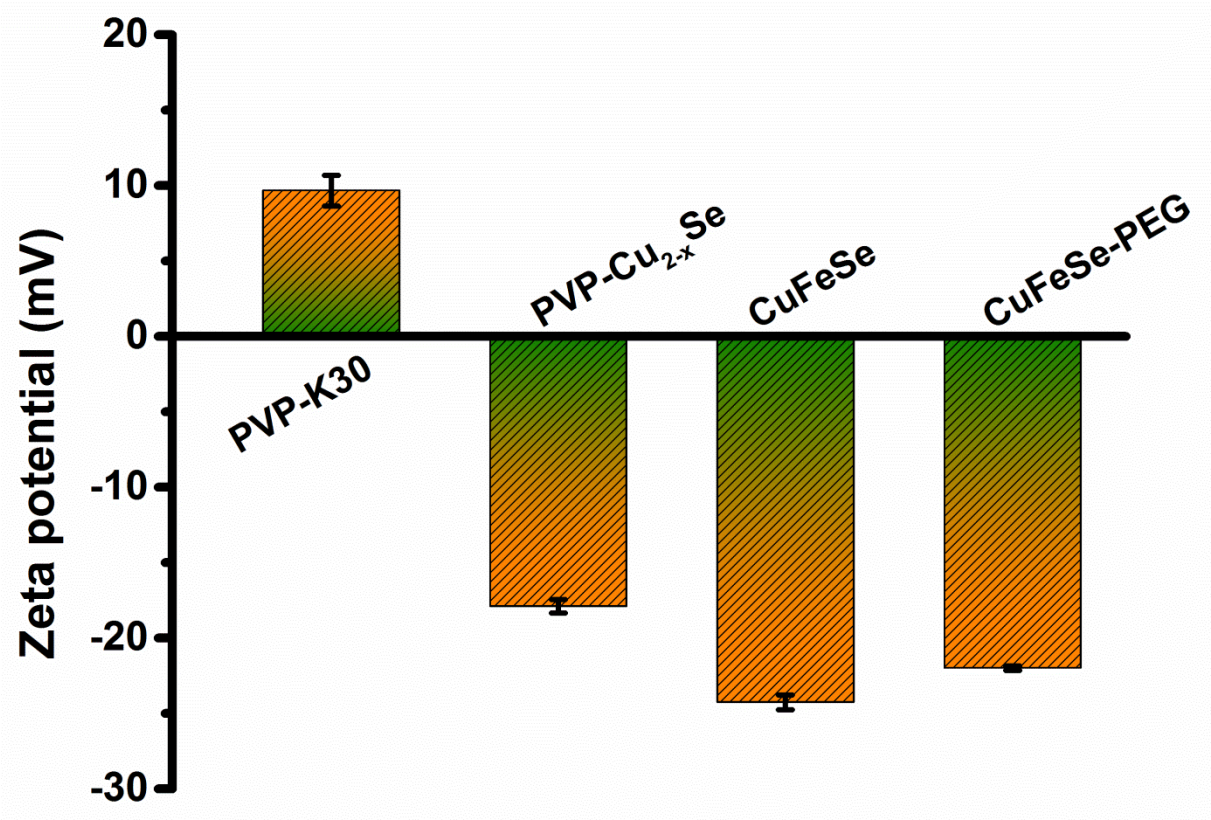

Figure S12. Zeta potentials of solutions of PVP-K30, PVP-$Cu_{2-x}Se$ NPs, CuFeSe NPs and CuFeSe-PEG NPs.

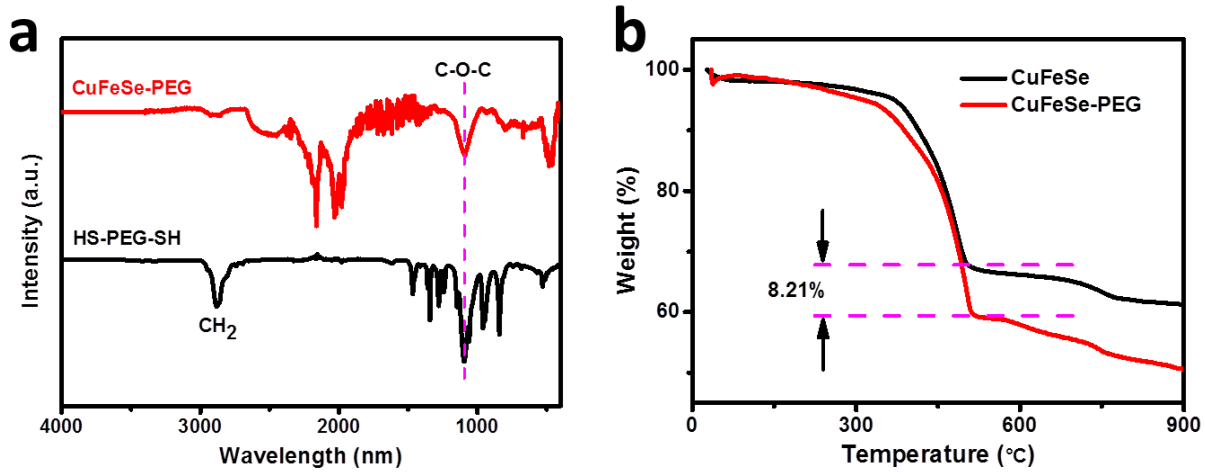

Figure S13. (a) FTIR spectra of the HS-PEG-SH and CuFeSe-PEG NPs, and (b) TGA curves of CuFeSe NPs recorded before and after PEG modification.

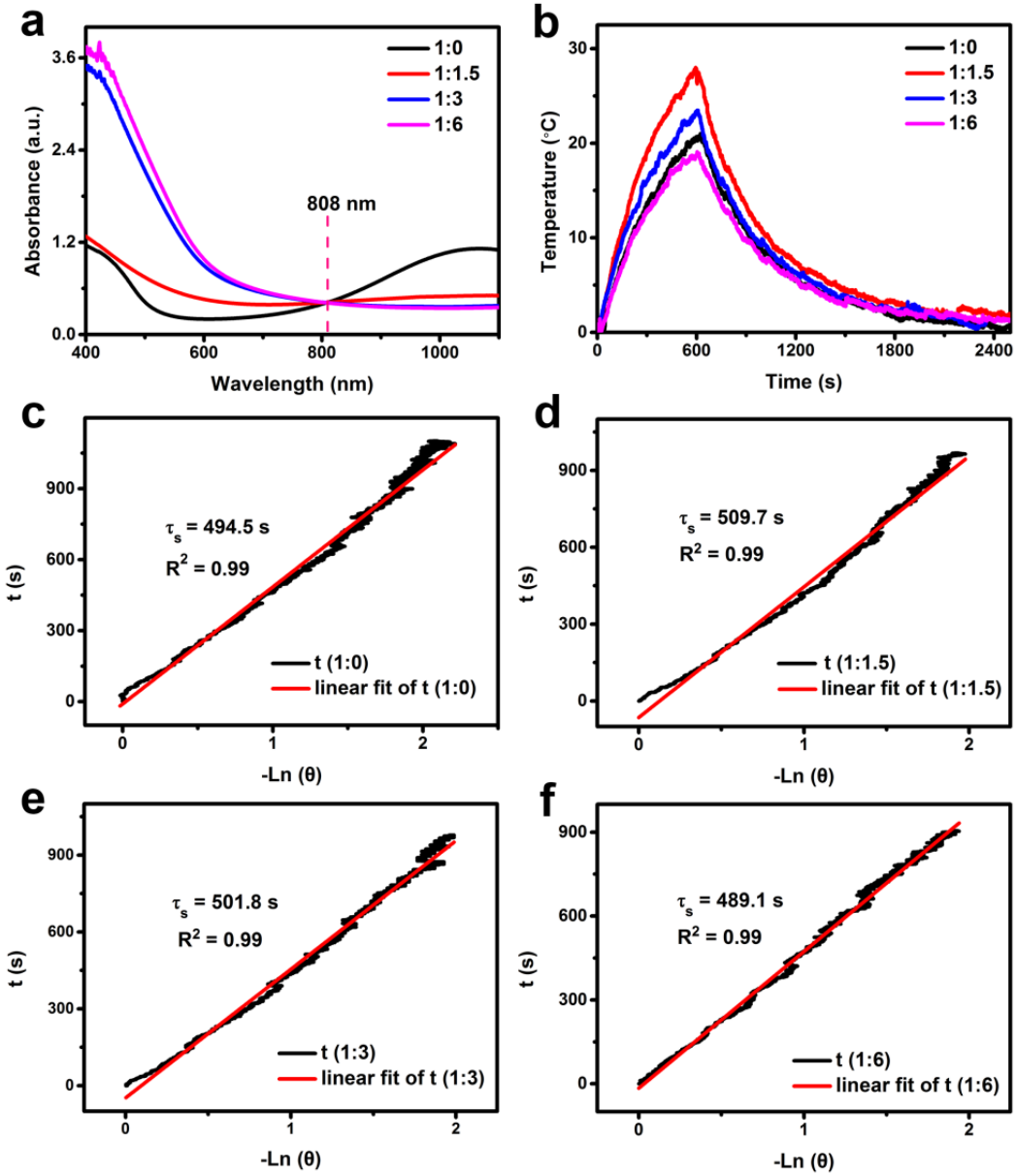

Figure S14. (a) UV-vis-NIR absorbance spectra of $Cu_{2-x}Se$ NPs and CuFeSe-PEG NPs prepared from different ratios of $Cu_{2-x}Se$: $FeCl_3$ with the same absorbance at 808 nm, (b) the photothermal conversion curves of $Cu_{2-x}Se$ and different CuFeSe-PEG samples irradiated with a 808-nm laser, followed by natural cooling after the laser was turned off. Determination of the system time constant of (c) $Cu_{2-x}Se$ NPs and CuFeSe NPs obtained from different $Cu_{2-x}Se$: $FeCl_3$ ratios, *i.e.*, (d) 1: 1.5; (e) 1: 3; and (f) 1: 6, by using linear regression of the cooling profiles shown in (b) respectively.

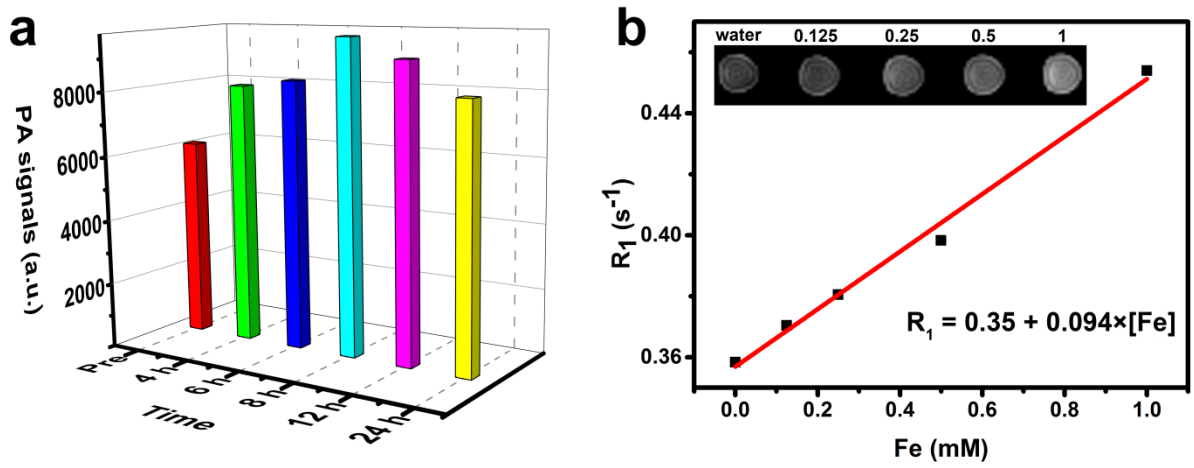

Figure S15. (a) *In vivo* PA intensity of tumor determined at different time points, and (b) *in vitro* T_1-weighted magnetic resonance (MR) imaging using different concentrations of CuFeSe-PEG NPs. The longitudinal (r_1) relaxivity was determined to be 0.10 mM^{-1} S^{-1}. Inset: the corresponding MR images.

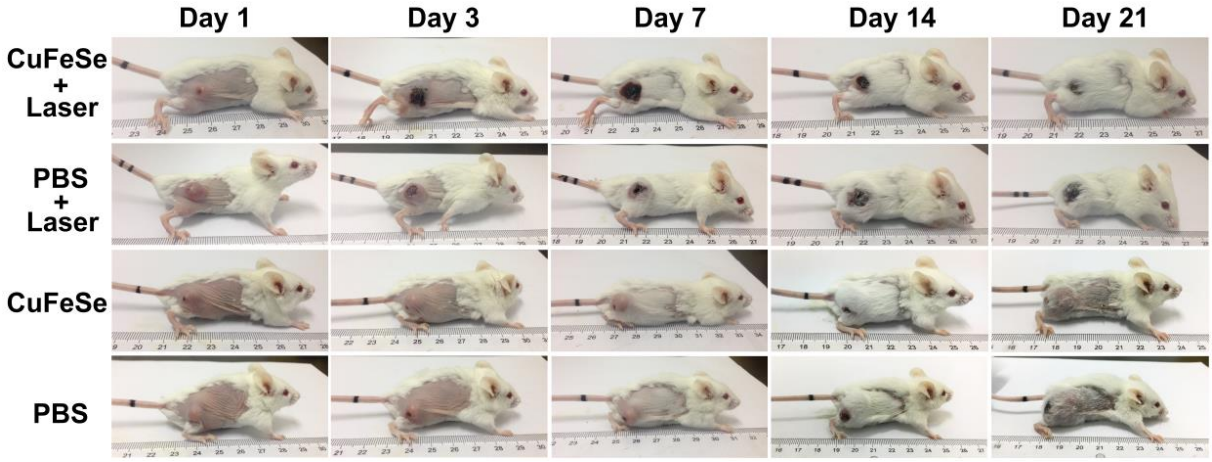

Figure S16. Representative images of mice taken at different times of post-treatment.

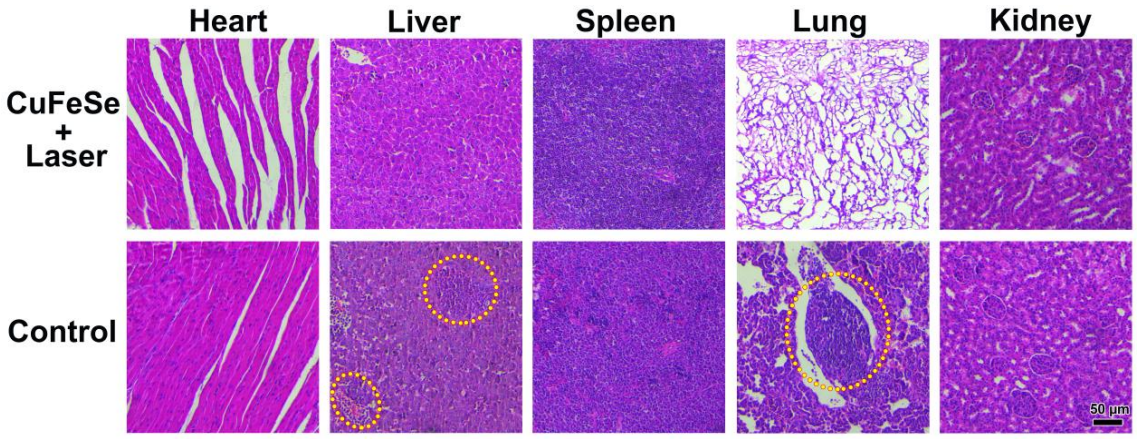

Figure S17. Representative H&E stained images of major organs from mice treated with intravenous injection of CuFeSe-PEG NPs (top row) and control mice (bottom row), harvested at 30 days after photothermal therapy. Yellow circles represent tumor metastasis regions.

[1] X. Ding, C. H. Liow, M. Zhang, R. Huang, C. Li, H. Shen, M. Liu, Y. Zou, N. Gao, Z. Zhang, Y. Li, Q. Wang, S. Li, J. Jiang, *J. Am. Chem. Soc.* **2014**, 136, 15684.